
COMPLETEDT: POINT CLOUD COMPLETION WITH DENSE AUGMENT INFERENCE TRANSFORMERS

A PREPRINT

Jun Li, Shangwei Guo, Shaokun Han*

Beijing Key Lab for Precision Optoelectronic Measurement Instrument and Technology, Beijing Institute of Technology
School of Optics and Photonics, Beijing Institute of Technology
Beijing, 100081, China
skhan@bit.edu.cn(* indicates the corresponding author)

June 13, 2022

ABSTRACT

Point cloud completion task aims to predict the missing part of incomplete point clouds and generate complete point clouds with details. In this paper, we propose a novel point cloud completion network, namely CompleteDT. Specifically, features are learned from point clouds with different resolutions, which is sampled from the incomplete input, and are converted to a series of *spots* based on the geometrical structure. Then, the Dense Relation Augment Module (DRA) based on the transformer is proposed to learn features within *spots* and consider the correlation among these *spots*. The DRA consists of Point Local-Attention Module (PLA) and Point Dense Multi-Scale Attention Module (PDMA), where the PLA captures the local information within the local *spots* by adaptively measuring weights of neighbors and the PDMA exploits the global relationship between these *spots* in a multi-scale densely connected manner. Lastly, the complete shape is predicted from *spots* by the Multi-resolution Point Fusion Module (MPF), which gradually generates complete point clouds from *spots*, and updates *spots* based on these generated point clouds. Experimental results show that, because the DRA based on the transformer can learn the expressive features from the incomplete input and the MPF can fully explore these feature to predict the complete input, our method largely outperforms the state-of-the-art methods.

Keywords 3D Point Cloud · Completion · 3D reconstruction · Transformer

1 Introduction

Point cloud data is one of the most popular 3D shape representations to express the attributes of real-world objects. 3D sensors such as LiDAR and Kinect are widespread used in point cloud acquisition process. However, the main limitations of these sensors are their resolutions and viewing angles, so geometric information may be not accurately acquired or even lost, which leads to incomplete and sparse point clouds[Huang et al., 2020]. Therefore, of particular concern is the 3D shape completion by learning the potential features of incomplete point clouds and then generating complete point clouds. The task of point cloud completion contributes to downstream 3D computer vision (CV) tasks like classification[Qi et al., 2017a,b], segmentation[Lei et al., 2020, Xu and Lee, 2020] and target detection[Ali et al., 2018, Chen et al., 2017].

In recent years, attention has been focused on point cloud completion tasks, which predict the missing shapes and maintain fine-grained complete shapes. The main concept is to learn the geometric properties and apparent structures to complete the point cloud. Some works[Dai et al., 2017, Yang et al., 2017] propose to perform the 3D convolution on voxels by voxelizing the point cloud. However, with the increase of the voxel resolution, these methods suffer from a heavy computational cost. Compared to the above methods voxelizing the point cloud, an increasing number of methods[Mandikal and Radhakrishnan, 2019, Yuan et al., 2018, Achlioptas et al., 2018, Groueix et al., 2018, Sarmad et al., 2019] based on PointNet[Qi et al., 2017a] and PointNet++[Qi et al., 2017b] directly process 3D coordinates to

complete the point cloud, which greatly save the computational cost. Point Cloud Completion (PCN)[Yuan et al., 2018], as the pioneer work based on PointNet[Qi et al., 2017a], adopts an encoder-decoder framework to decode a complete shape from global features extracted by the encoder. However, PCN[Yuan et al., 2018] has failed to benefit from local features, and can't generate fine geometric details. Other methods[Wang et al., 2020a, Wen et al., 2020, 2021] explore the usefulness of the local information to improve the performance of point cloud completion. Local features can express the structure information by relating points and their neighborhood points. For example, SA-Net[Wen et al., 2020] exploits the local details by a skip-attention mechanism, which can selectively emphasize geometric information from the local regions for the generation of complete point clouds.

The current methods[Wang et al., 2020a, Pan, 2020] imitate the visual 2D Convolutional Neural Network (2D-CNN) to build a hierarchical network, where each layer extracts local features from neighbors. As the network deepens and the receptive field increases, it aggregate local features to global features. Because of the imitation of 2D-CNN, these methods inherit drawback of 2D-CNN, that is, the lack of ability to extract global features. The global features can express the information of the entire point cloud, and can provide important semantic contexts. Thus, it is important to use global features in the procession of point cloud completion. However, the transformer[Vaswani et al., 2017] aggregates information from the entire point cloud to output features, so it has a global receptive field to extract the global features of the point cloud. To learn local detail features while exploring global features, hence improving the performance of point cloud completion, we propose a network based on the transformer[Vaswani et al., 2017], named CompleteDT. Our model is structured in four components: **1) ResMLP Module:** ResMLP Module extracts features by performing linear transformation at point level. To fully extract features from the point cloud to complete the incomplete input, multi-resolution feature maps are obtained from these features with Iterative Farthest Point Sampling (IFPS). **2) Self-Guided Relation Module (SGR):** The local information of point clouds plays an important role for point cloud completion. The SGR is designed to aggregate local information from multi-resolution feature maps and to sequentially process these feature maps from low to high resolution to generate *spots* with multiple resolutions, which contain local information and semantic contexts. **3) Dense Relation Augment Module (DRA):** To further extract the local information and explore global relationships between *spots*, we design the DRA, which is based on the transformer[Vaswani et al., 2017]. This module is composed of two key components, i.e., Point Local Attention Module (PLA) and Point Dense Multi-Scale Attention Module (PDMA). PLA adaptively learns local features only from neighbors around *spots*. PDMA can densely extract the global correlation among all *spots*. It divides the multi-head attention into different groups. Each group receives the set of the outputs of all previous groups and aggregates them to a representation with an embedding dimension. This design makes the structure of PDMA quite different from that of the transformer[Vaswani et al., 2017]. DRA adopts PLA and PDMA in parallel to extract the global information and retain local features. **4) Multi-resolution Point Fusion Module (MPF):** We devise a multi-resolution generation module for completing point clouds in a coarse-to-fine manner. MPF first generates *global spots*, which represent the information about the complete shape, and then uses *spots* at different semantic levels to progressively generate complete shapes with different resolutions and update *global spots*. Finally, the updated *global spots* can be used to recover the final complete point cloud.

Our main contributions can be summarized as follows:

- We propose a novel module DRA consisting PLA and PDMA, which extracts adequate features containing local information and global semantics. PLA enhances to inference the local information of *spots*. PDMA, where embedding dimensions of kernels of multi-head attention are different, extracts the global correlation among all *spots*. Thus, DRA provides detailed local information and global correlations for the Multi-resolution Point Feature Fusion to generate a complete point cloud.
- We propose the MPF to generate a high-quality complete point cloud in the way that the spatial position of points control distribution of features. Specifically, it first generates a complete point cloud on an unorganized sets of 3D feature maps, and then updates the features based on the spatial structure of this point cloud, thereby forcing the geometric mapping of the point cloud onto the feature space.
- We propose a novel network CompleteDT for point cloud completion task. CompleteDT can learn local features within each spot and explore the global correlation among *spots*. Compared with previous methods of point cloud completion, CompleteDT achieves the state-of-art performance of point cloud completion.

2 Related Work

2.1 3D Shape Completion

Based on voxel data Due to the unordered property of point clouds, some methods[Dai et al., 2017, Yang et al., 2017, Wang et al., 2019, Han et al., 2017, Nguyen et al., 2016, Stutz and Geiger, 2018, Varley et al., 2017] voxelize point

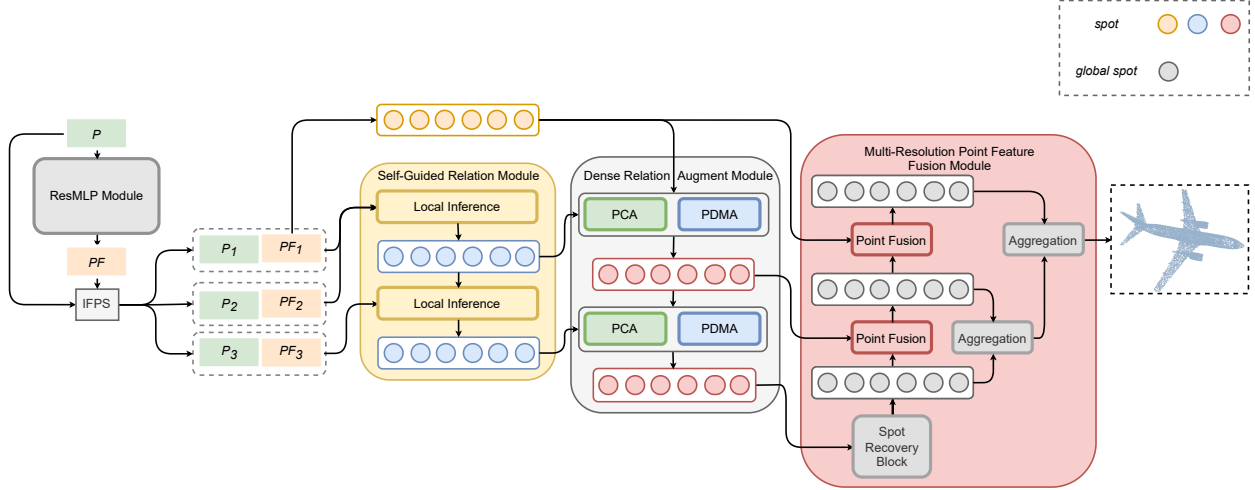


Figure 1: The overall architecture of CompletedDT, which consists of four modules: ResMLP Module, Self-Guided Relation Module, Dense Relation Augment Module and Multi-resolution Point Fusion Module. We first use ResMLP Module based on MLP to extract features. Then multi-resolution point clouds and their features are obtained. After obtaining *spots* (blue circle) with Self-Guided Relation Module, we use a transformer-based module to enhance the inference of *spots* (red circle). Finally, we obtain *global spots* (gray circle) and gradually update them to generate the complete point cloud.

clouds into rigid grids and then perform 3D convolution on them. For example, the 3D-Encoder-Predictor Network (3D-EPN)[Dai et al., 2017] generates a low-resolution complete output, and then refines it from a shape database. Although the voxel-based method can complete the shape, its details are lost for the introduced quantization error, and its computational cost increases significantly with increasing resolution.

Based on point cloud data To solve the unordered structure of point cloud, PointNet[Qi et al., 2017a] is proposed to analyze point clouds on point level and has benefited to many downstream tasks. For point cloud completion, PCN[Yuan et al., 2018], as the pioneer work based on PointNet[Qi et al., 2017a] for completing the point cloud, extracts the global representation from the incomplete point cloud and then decodes this representation to generate the point cloud from coarse to detail. However, the point cloud generated by PCN[Yuan et al., 2018] lacks details due to ignoring local information. After PCN[Yuan et al., 2018], other methods emerge and recover the point cloud with the higher resolution. For example, PF-Net[Huang et al., 2020] is an encoder-decoder network based on the Adversarial Generative Networks (GAN). PF-Net[Huang et al., 2020] suggests to predict the missing shape of the input instead of generating the overall shape, and then forms the complete shape with the missing shape and the input. PF-Net[Huang et al., 2020] can well retain the spatial arrangements of the input and figure out the detailed geometrical structure in missing. VRCNet[Pan et al., 2021] is the first network for point cloud completion based on the probabilistic model. VRCNet[Pan et al., 2021] first predicts the coarse shape with “probabilistic modeling” (PMNet) and then recovers shape details with “relational enhancement” (RENet). GRNet[Xie et al., 2020] refocus on the voxel data for its rigid structure. GRNet[Xie et al., 2020] introduces 3D grids as an intermediate representation to generate the complete point cloud, thereby recovering the structural and context information of the point cloud. SoftPoolNet[Wang et al., 2020b] generates high-resolution complete point cloud by sorting features into a feature map to obtain local groups and then applying the 2D convolution. Based on the SoftPoolNet[Wang et al., 2020b], SoftPool++[Wang et al., 2022], as a feature extraction module, can be applied multiple times in an encoder-decoder architecture by the use of point-wise skip connections. Based on the above design, model based on SoftPool++[Wang et al., 2022] can generate complete point clouds that preserve geometric details.

2.2 Transformer on 3D Point Cloud

Transformers[Vaswani et al., 2017] are first applied in the field of Natural Language Processing (NLP), and process data in parallel and order-independent. Transformers[Vaswani et al., 2017] can extract long-range features due to its capability of aggregating global features. The subsequent success[Devlin et al., 2018, Liu et al., 2021, Rao et al., 2021] of transformers[Vaswani et al., 2017] in computer vision (CV) greatly aroused transformer’s interest in the field of 3D point clouds. Based on the transformer[Vaswani et al., 2017], a new learning framework PCT[Guo et al., 2021] is proposed. PCT[Guo et al., 2021] first extracts local features from grouped points and then inputs these local features

to the module based on the transformer[Vaswani et al., 2017] for learning the global representation. In the realm of point cloud completion, PMP-Net++[Wen et al., 2022], introduces a self-attention transformer[Vaswani et al., 2017] module between each set abstraction (SA) layer of PointNet++[Qi et al., 2017b] based encoder, strictly learns the correspondence at the point level and moves each point of the incomplete input to improve the quality of the complete point cloud. CompleteDT benefits from transformer[Vaswani et al., 2017] to augmenting the inference of features. One striking characteristic of our approach is that we use a transformer based on a self-attention mechanism with kernels embedding different dimensions, which can ensure the effective fusion of features at semantic information. PoinTr[Yu et al., 2021] converts the point cloud to a sequence of point proxies and devises a transformer-based block that completes the shape. PoinTr[Yu et al., 2021] first exploits the self-attention mechanism to explore long-range semantic correlations, then uses a linear layer to learn local geometric information on local proxies captured by K-nearest neighbor (KNN). Finally, these two kinds of results are fused to ensure global information and local information, and recover detailed information for point cloud completion. The difference exists between PoinTr[Yu et al., 2021] and CompleteDT is that CompleteDT is concerned with the performance of transformers[Vaswani et al., 2017] on local information and designs the PLA (Section 3.4) to learn the local information, while PoinTr[Yu et al., 2021] focuses on the description of local information with KNN. CompleteDT adaptively measures neighborhood weights to better infer local information. The ablation study (Section 5.2) proves the efficiency of the PLA.

3 Methods

In this section, we first introduce the proposed model CompleteDT, which can learn useful features from incomplete point clouds and then infer complete shapes. Next, we show the mentioned modules separately. Finally, we present loss functions.

3.1 Model

Our goal is to complete the point cloud with more details by extracting the features within neighborhoods of the point cloud and exploring the interaction among these neighborhoods. It may be insufficient to only integrate local features while ignoring the global relationship among neighborhoods[Cui et al., 2021]. However, the difficulty in the extraction of global relationship exists because local features within receptive fields is extracted layer by layer and then global information is aggregated from these local features as the network deepens and receptive fields increases. The recent success in the transformer[Vaswani et al., 2017] has clearly demonstrated the effectiveness of resolving the disorder of point clouds and extracting long-range features. Thus, we propose a network based on the transformer[Vaswani et al., 2017] for point cloud completion.

As shown in Figure 1, we first use the ResMLP Module as preprocess (Section 3.2) to extract features from the input and then obtain multi-resolution point clouds and multi-resolution feature maps with IFPS. Then, we design the Self-Guided Relation Module (SGR) (Section 3.3) to obtain the *spots* by aggregating local information from multi-resolution feature maps and then sequentially processing these feature maps from low to high resolution. To be further infer the *spots* to improve the performance of point cloud completion, we present the Dense Relation Augment Module (DRA) (Section 3.4) consisting of the Point Local Attention Module (PLA) and the Point Dense Multi-Scale Attention Module (PDMA). The PLA can enhance the inference of features within the *spots*. The PDMA considers information of *spots* from different resolution point clouds comprehensively. Concretely, the *spots* from high-resolution point cloud contain more detailed information, while *spots* from low-resolution point cloud tends to retain the knowledge of overall geometry. Therefore, outputs of two kinds of modules are fused to obtain the representation with both long-range and short-range information. Based on expressive features learned from DRA, we design the Multi-resolution Point Fusion Module (MPF) (Section 3.5) to generate a high-resolution complete shape. Specifically, it first generates *global spots* containing global information of a complete shape, then obtains multi-resolution point clouds and updates *global spots* based on the spatial structure of these point clouds. Spatial positions of point clouds is forced to map onto the distribution of *global spots*. The updated *global spots* can be used to generate the final complete shape with the high resolution.

3.2 ResMLP Module

As one of the most well-known methods for point cloud analysis, PointNet[Qi et al., 2017a] proposes to directly process 3D coordinates of points with multi-layer perceptron layers (MLP). MLP facilitates the transformation of features for its simple nature and the powerful representation capability[Xie et al., 2020]. Inspired by this idea, we present a module named ResMLP Module based on the residual mechanism. ResMLP is a pre-processor to extract features on each point, and the architecture of it is shown in Figure 2. Specifically, given a point cloud $P \in \mathbb{R}^{N \times 3}$, we perform two MLP

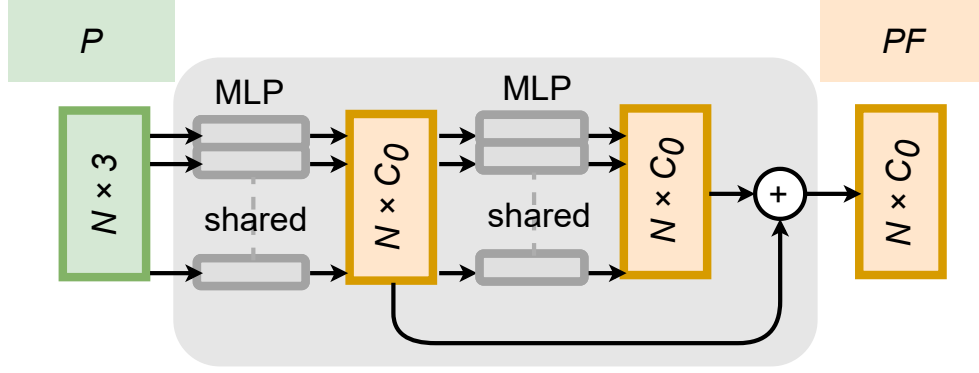


Figure 2: Illustration of the ResMLP Module, which mainly consists of two MLP layers.

layers sequentially on this point cloud P and then sum these results in pairwise with the skip connection as the final output $PF \in \mathbb{R}^{N \times C_0}$ ($C_0 = 64$).

Due to the shape of P is incomplete, features can only be inferred from the visible shape of P . To extract as much geometry knowledge as possible from P , we propose to sample point clouds [Qi et al., 2017b] to get multi-resolution feature maps. Features of a high-resolution point cloud can provide detail information. Although features of a low-resolution point cloud may ignore the details, they are closer to the overall skeleton features. As shown in Figure 1, we obtain multi-resolution point clouds $P_m \in \mathbb{R}^{N_m \times 3}$ ($m = 1, 2, 3, N_1 > N_2 > N_3$) and feature maps $PF_m \in \mathbb{R}^{N_m \times C_0}$ by sampling P and PF with IFPS.

3.3 Self-Guided Relation Module

To take full advantage of the multi-resolution point clouds P_m and their feature maps PF_m , we design the Self-Guided Relation Module (SGR) for gradually fusing local features in a self-guided way. SGR uses the hierarchical relationship of point clouds with different resolutions to sequentially aggregates features. Considering the hierarchical relationship ensures that the high-resolution information provides local details for the low-resolution information, while the features of the low resolution guide the integration of high-resolution features. As a result, semantic information is enhanced due to features being aggregated in a hierarchical manner. Therefore, it is effective for fusing features to consider hierarchical relationships.

For two point clouds with different resolution, the local information of a point in the lower one can be provided by the higher one. This point in the low-resolution point cloud and its local features in the high-resolution point cloud can be defined as a *spot*. As shown in Figure 3 (a), we consider the output of m_{th} stage of SGR as $spots^m$. PF_2 guides the fusion of PF_1 to obtain $spots^2$ with Local Inference, which is an efficient block of SGR. Then the $spots^2$ propagates its information to PF_3 to generate $spots^3$. Especially, $spots^1$ indicates features PF_1 .

Figure 3 (b) shows the details of Local Inference. Taking any two sets of $\{P_m, PF_m\}$ and $\{P_{m+1}, PF_{m+1}\}$ as an example, we implement grouping operation proposed by PointNet++ [Qi et al., 2017b] to capture local features. Simply, for $p_i \in P_{m+1}$, we first gather its neighborhoods N_K (Eq. 1), and then obtain its neighbor points $P^G \in P_m$ and their features $PF^G \in PF_m$ (Eq. 2).

$$N_K(p_i, P_m) = \{k \mid d(p_i, p_k) < r, p_k \in P_m\} \quad (1)$$

where, $d(\cdot)$ is a distance function and r is the threshold.

$$\begin{aligned} P^G &= \bigcup_{k \in N_K(p_i, P_m)} p_k \in P_m \\ PF^G &= \bigcup_{k \in N_K(p_i, P_m)} pf_k \in PF_m \end{aligned} \quad (2)$$

In addition to being the input of grouping operation, PF_{m+1} also needs to map its dimensions to PF_m . Then, we obtain the relative relationship by subtracting between P_m and P^G in the channel dimension. After concatenating these representations on the channel dimension, we obtain $spots^{m+1}$ from two sets of $\{P_m, PF_m\}$ and $\{P_{m+1}, PF_{m+1}\}$ by

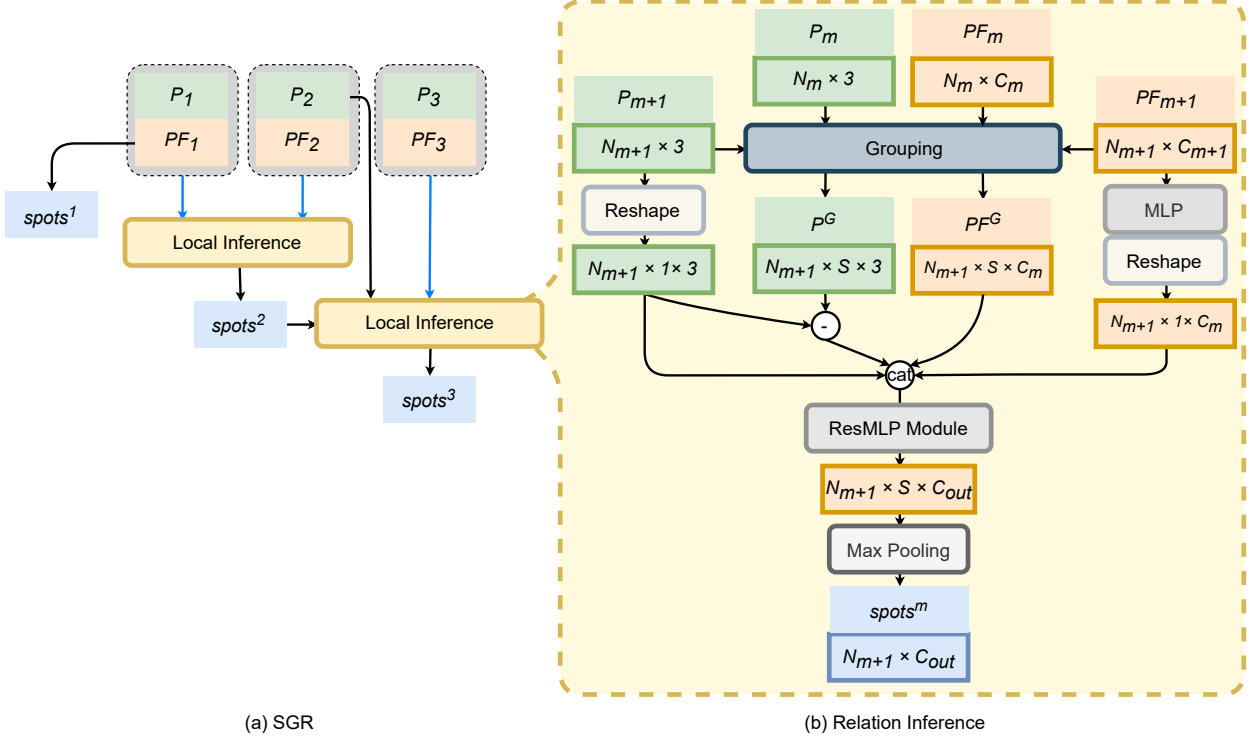


Figure 3: Illustration of the Self-Guided Relation Module, which is responsible for generating $spots^1$, $spots^2$ and $spots^3$. $spots^1$ indicates features PF_1 , $spots^2$ and $spots^3$ mean features obtained by Local Inference. The blue arrow indicates that the set of $\{P_m, PF_m\}$ inputs to Local Inference. The superscript ‘‘G’’ means ‘‘Group’’

using the ResMLP Module (Section 3.2) and the Max-pool layer. Therefore, $spots^{m+1}$ contain the details of PF_m and the semantic features of PF_{m+1} . Then $spots^{m+1}$ are used to aggregate its own information into PF_{m+2} to generate $spots^{m+2}$. In this way, SGR aggregates features sequentially based on hierarchical relationships and generates $spots$ containing local information.

3.4 Dense Relation Augment Module

The $spots^m$ generated from SGR(Section 3.3) contain local information. It may be insufficient to consider local information. The global correlation between any two $spot_i, spot_j \in spots^m$ ($i \neq j$) should be taken into account. However, the common operation like convolution is restrictive in acquiring global correlation. The transformer[Vaswani et al., 2017] contributes to solve this problem for its ability of obtaining long-range information for the processing of any feature. Based on the transformer, we design a valid module, named Dense Relation Augment Module (DRA). In this section, we first review the transformer[Vaswani et al., 2017], then introduce DRA and its important components.

3.4.1 Review of the transformer

One interpretation of transformers applied to point clouds is to regard the point cloud as a sentence and its point as words[Guo et al., 2021]. The common form of transformer is based on self-attention mechanism. Given the input $F \in \mathbb{R}^{N \times C_F}$, it is performed by a the linear transformations with kernel weights W_q, W_k, W_v to finish the self-attention mechanism. We use the symbol \mathcal{H} to represent the operation of self-attention mechanism:

$$f = \mathcal{H}(F, W_q, W_k, W_v) \quad (3)$$

where $W_q \in \mathbb{R}^{C_F \times C}$, $W_k \in \mathbb{R}^{C_F \times C}$ and $W_v \in \mathbb{R}^{C_F \times C}$ are shared learnable parameters

F is projected into the query $Q \in \mathbb{R}^{N \times C}$, key $K \in \mathbb{R}^{N \times C}$ and value $V \in \mathbb{R}^{N \times C}$ with the linear transformations[Vaswani et al., 2017]:

$$Q, K, V = F \otimes W_q, F \otimes W_k, F \otimes W_v \quad (4)$$

where ‘‘ \otimes ’’ represents the matrix multiplication.

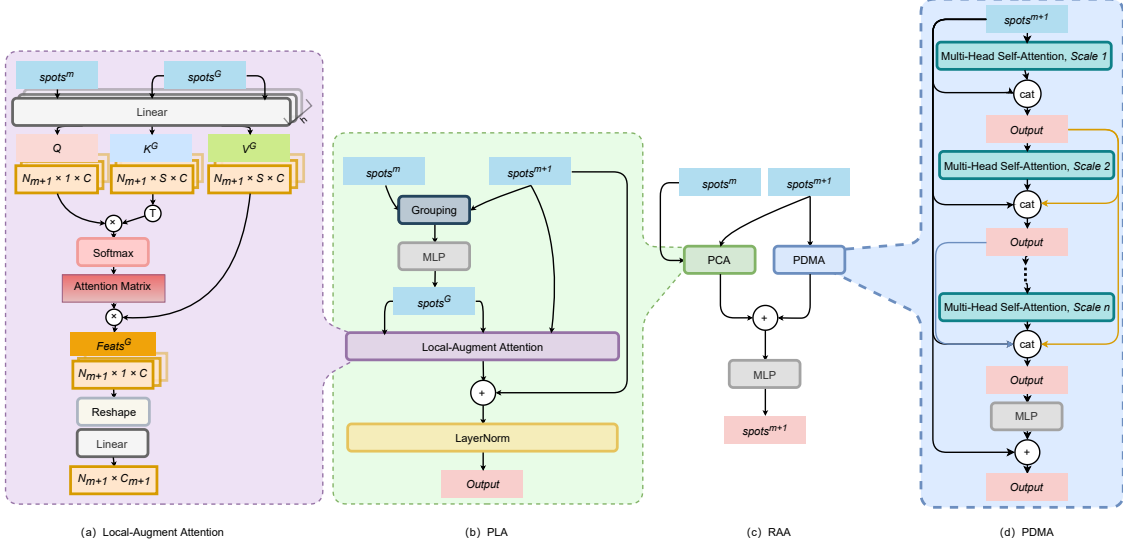


Figure 4: Illustration of the m_{th} stage of Dense Relation Augment Module. This module consists of PLA (b) and PDMA (d). PLA is composed of the Local-Augment Attention (a).

The specific operation process is shown in Figure 5 (a). The attention matrix $A \in \mathbb{R}^{N \times N}$ is generated by performing the matrix multiplication on Q and K , normalizing and applying softmax function sequentially. The $a_i^j \in A$ can be expressed as Eq. 5.

$$a_i^j = \text{softmax}\left(\frac{\sum_{c=1}^C q_i^c k_j^c}{\sqrt{d_s}}\right) \quad (5)$$

where $q_i \in Q$, $k_j \in K$, and d_s is the value of normalization.

The attention matrix A is multiplied by V to obtain $Feats$. The feature $f_i^c \in Feats$ can be expressed as follows:

$$f_i^c = \sum_{n=1}^N \alpha_i^n v_n^c \quad (6)$$

where $v_n^c \in V$. The letter “ C ” means the number of the channel dimension. The letter “ N ” indicates the number of point cloud.

3.4.2 The architecture of DRA

Based on the self-attention mechanism, we design a valid module, named Dense Relation Augment Module (DRA). Our DRA consists of Point Local-Attention Module (PLA) and Point Dense Multi-Scale Attention Module (PDMA). DRA adopts the same feature aggregation method as SGR (Section 3.3), which tries to further infer local information of $spots$ based on hierarchical dependencies. For the convenience of explanation, we take m_{th} stage of DRA as an example. For $spots^m$ and $spots^{m+1}$, DRA utilizes PLA and PDMA in parallel to boost the feature inference procession. As shown in Figure 4 (c), PLA facilitates to extract the local information by fusing features of $spots^m$ into that of $spots^{m+1}$, and PDMA favors to obtain the global correlation among all elements of $spots^{m+1}$. Obtaining the output of DRA first sums the results of PLA and PDMA in pairwise and then applies the MLP layer. In this way, $spots^{m+1}$ are updated by DRA not only contains local information, but also supplements global dependencies.

3.4.3 The architecture of PLA

PLA migrates the transformer’s property of learning long-range features to local features and measures weights of local information adaptively. As shown in Figure 4 (b), PLA, including the Local-Augment Attention (Figure 4 (a)), is an attention module based on residual block for strengthening the inference of local features. For the $spots^{m+1} \in \mathbb{R}^{N_{m+1} \times C_{m+1}}$, we obtain $spots^G \in \mathbb{R}^{N_{m+1} \times S \times C_m}$ by gathering its neighborhood $spots$ from $spots^m \in \mathbb{R}^{N_m \times C_m}$ ($N_m > N_{m+1}$)

based on neighborhoods N_K (Eq. 1) from SGR and applying the MLP. After obtaining $spots^G$, it and $spots^{m+1}$ input to the Local-Augment Attention.

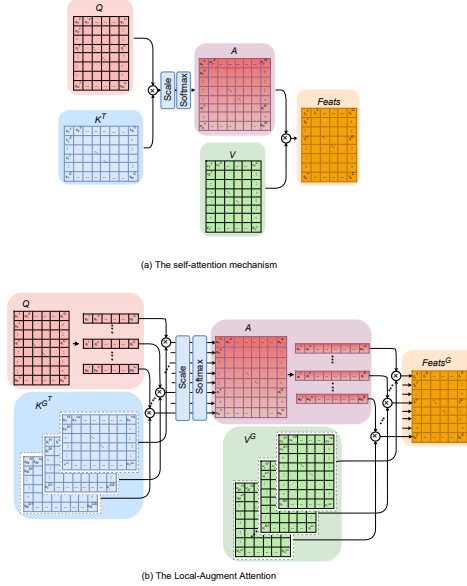


Figure 5: The specific implementation of the vanilla transformer and Local-Augment Attention. Scale means the normalized parameter.

Different from the self-attention that obtains semantic relation among all features, Local Augment Attention uses the feature similarity to capture the geometric correlation between a *spot* and its certain local *spots*. The specific implementation of our Local Augment Attention is shown in the Figure 5 (b). $spots^{m+1}$ is used to obtain queries $Q \in \mathbb{R}^{N \times 1 \times C}$, and $spots^G \in spots^m$ is used to get keys $K^G \in \mathbb{R}^{N \times S \times C}$ and values $V^G \in \mathbb{R}^{N \times S \times C}$. Eq. 4 becomes:

$$\begin{aligned} Q &= spots^{m+1} \otimes W_q \\ K^G, V^G &= spots^G \otimes W_k, spots^G \otimes W_v \end{aligned} \quad (7)$$

where $W_q \in \mathbb{R}^{C_{m+1} \times C}$, $W_k \in \mathbb{R}^{C_m \times C}$ and $W_v \in \mathbb{R}^{C_m \times C}$ are shared learnable linear parameters. “ \otimes ” represents the matrix multiplication.

We compute the products of Q with K^{G^T} , and apply normalization and softmax function to obtain the attention matrix A , that is weights of V^G . For $a_i^j \in A$ is computed similarly to Eq. 5:

$$a_i^j = softmax\left(\frac{\sum_{c=1}^C q_i^c k_i^{c_j}}{\sqrt{d_s}}\right) \quad (8)$$

where $q_i^c \in Q$, $k_i^{c_j} \in K^{G^T}$. The letter “ C ” means the number of the channel dimension.

The attention matrix A is multiplied by V^G to obtain $Feats^G$. For $f_i^c \in Feats^G$, it can be expressed as follows:

$$f_i^c = \sum_{s=1}^S a_i^s v_i^{s_c} \quad (9)$$

where $v_i^{s_c} \in V^G$. The letter “ C ” means the number of the channel dimension. The letter “ S ” indicates the number of local *spots*.

The results of Local-Augment Attention are obtained by performing a linear transformation on $Feats^G$ to map its dimension to the original $spots^{m+1}$. Finally, based on Residual mechanism, the original $spots^{m+1}$ convey their features to these results to obtain the output of PLA.

PLA concludes a further inference about $spots^{m+1}$ and emphasizes semantic information by utilizing their neighbors $spots^G \in spots^m$.

3.4.4 The architecture of PDMA

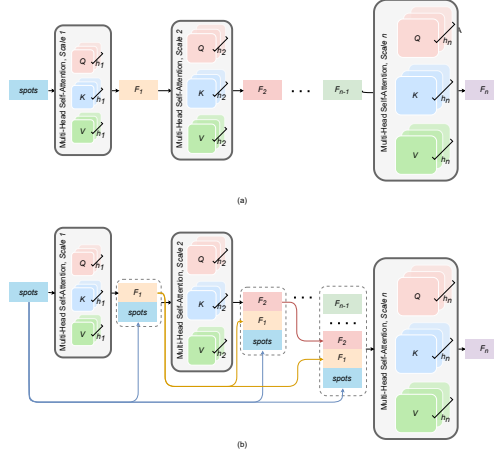


Figure 6: Visualization of the architecture of PDMA, (a) shows the multi-scale attention and (b) indicates the multi-scale attention with dense connection, $h_1 = h_2 = \dots = h_n$.

PLA promotes the inference of neighborhood information and updates each *spot* by adaptively measuring the weights of the neighborhood features. However, different interactions of various *spots* are not taken into account, which may not aggregate global information among *spots* well. Therefore, it is necessary to explore the semantic information of *spots*. To explore relationships among these *spots*, we present Point Dense Multi-Scale Attention Module (PDMA) (Figure 4 (d)). Although a vanilla transformers[Vaswani et al., 2017] is competent at the task of extracting correlations of *spots*, our goal is to improve the representation of *spots* by dynamically aggregating them depending on their semantic content.

The vanilla transformers[Vaswani et al., 2017] has h heads, and the shapes of $\{Q, K, V\}$ of all heads are the same. Different from the vanilla transformers[Vaswani et al., 2017], our PDMA divides h heads into n groups, the shapes of $\{Q, K, V\}$ in each group are different. Figure 6 (a) visualizes shapes of Q, K and V of multi-scale attention. Output of the n_{th} group with a scale of sc_n can be learned from its previous group with a scale of sc_{n-1} . Eq 3 becomes:

$$F_n = \mathcal{H}(F_{n-1}, W_q^{sc_n}, W_k^{sc_n}, W_v^{sc_n}) \quad (10)$$

where F_{n-1} is the output of $(n-1)_{th}$ group.

We set the baseline of channel dimension as C ($C = 64$) and set the scale factor as sc_n ($sc_1 = 2, sc_2 = 4$). The $\{Q, K, V\}$ with the scale sc_n can be regarded as $\{Q^{sc_n}, K^{sc_n}, V^{sc_n}\}$. The representation of Q^{sc_n}, K^{sc_n} and V^{sc_n} of n_{th} group can be changed from Eq. 4 to:

$$\begin{aligned} Q^{sc_n} &= F_{n-1} \odot W_q^{sc_n}, \\ K^{sc_n} &= F_{n-1} \odot W_k^{sc_n}, \\ V^{sc_n} &= F_{n-1} \odot W_v^{sc_n} \end{aligned} \quad (11)$$

where F_{n-1} is the output of the $(n-1)_{th}$ group of PDMA, $W_q^{sc_n}, W_k^{sc_n}$ and $W_v^{sc_n}$ are shared learnable linear parameters with the shape of $[C_{F_{n-1}}, C^{sc}]$, $C_{F_{n-1}}$ is the channel dimension of F_{n-1} , $C^{sc_n} = C \times sc_n$.

To make full use of the features as much as possible, we also add the dense connection[Huang et al., 2017, Iandola et al., 2014, Liu et al., 2019]. As shown in Figure 6 (b), For the n_{th} group of PDMA, its input is the concatenation of outputs from all previous groups. Therefore, Eq. 10 can be modified as:

$$F_n = \mathcal{H}((F_0 \cdot F_1 \cdot \dots \cdot F_{n-1}), W_q^{sc_n}, W_k^{sc_n}, W_v^{sc_n}) \quad (12)$$

Similarly, Eq. 11 becomes:

$$\begin{aligned} Q^{sc_n} &= (F_0 \cdot F_1 \cdot \dots \cdot F_{n-1}) W_q^{sc_n} \\ K^{sc_n} &= (F_0 \cdot F_1 \cdot \dots \cdot F_{n-1}) W_k^{sc_n} \\ V^{sc_n} &= (F_0 \cdot F_1 \cdot \dots \cdot F_{n-1}) W_v^{sc_n} \end{aligned} \quad (13)$$

where F_0 is the original input *spots*, F_i ($i = 1, \dots, n-1$) is the outputs of n_{th} group of PDMA. " \cdot " means the concatenation operation.

In the end, results of all groups are spliced on the channel dimension, and the final output is obtained from these results spliced through MLP. PDMA sequentially aggregates different semantic information extracted from each group. As the PDMA deepens, representation is mapped to feature spaces with higher dimensional but information in lower dimensions may be lost. The dense connection approach complements the low-dimensional semantic context, aiding in recovering the details of the complete point cloud. PDMA achieves to extract the correlation among *spots*.

3.5 Multi-resolution Point Fusion Module

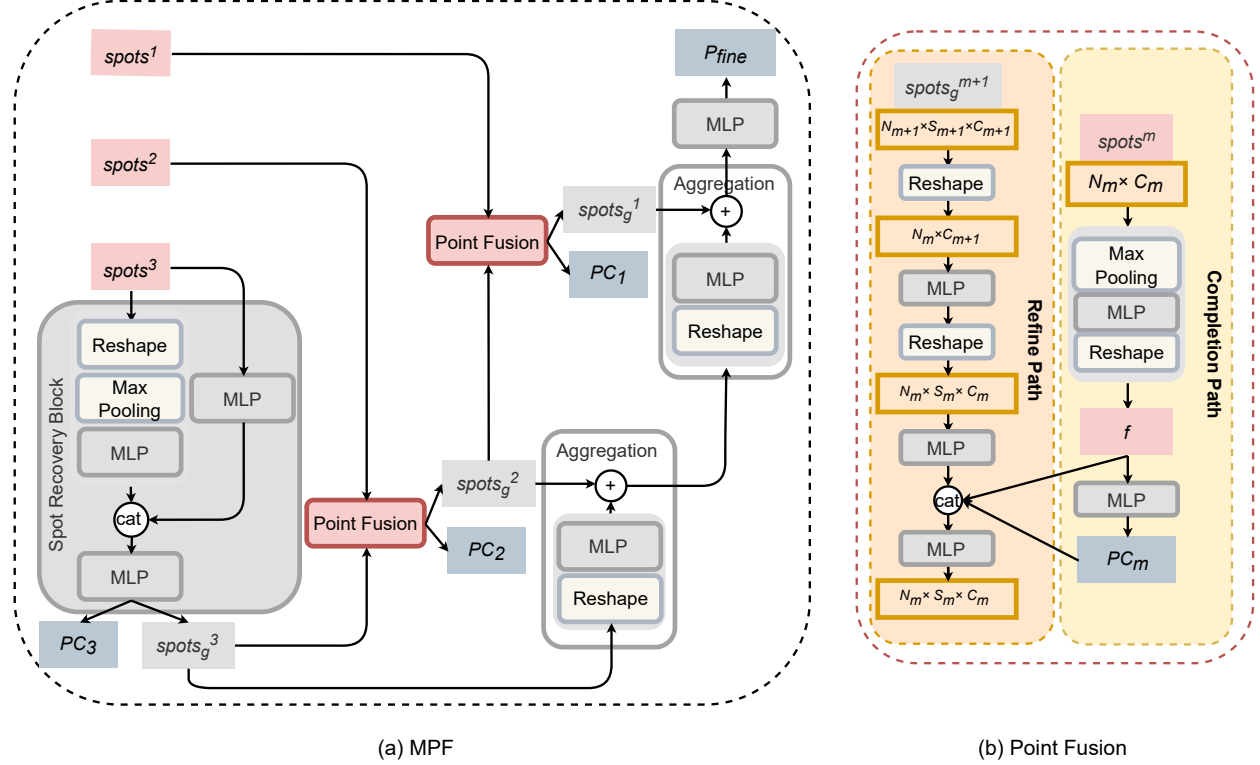


Figure 7: Illustration of the Multi-resolution Point Fusion Module and Point Fusion Block. The subscript “*g*” indicates “global”.

According to these modules designed above, we gradually obtain $spots^m$ ($m = 1, 2, 3$) from point clouds with different resolution. Each set of $spots$ has rich local information, and contains the global correlation. To recover a complete point cloud from these features, we propose the Multi-resolution Point Fusion Module (MPF) to complete a high-resolution point cloud. MPF first recovers *global spots* to represent the information of the complete shape, and then uses $spots$ with different semantic contexts to generate complete point clouds with multiple resolutions. Each point cloud forcibly to map its spatial structure to the feature space to update *global spots*. Therefore, under the restriction of the spatial location of the points, the distribution of the features matches that of the complete point cloud. For convenience of presentation, $spots_g^m$ denotes *global spots* in m_{th} stage of MPF.

As shown in Figure 7 (a), we follow the principle “from coarse to fine” to generate a complete shape. To begin with, $PC_3 \in \mathbb{R}^{N_3 \times 3}$ and $spots_g^3 \in \mathbb{R}^{N_3 \times S_3 \times C_3}$ are obtained from $spots^3$ by a Spot Recovery Block. PC_3 can be regards as skeleton points for grasping the complete shape and $spots_g^3$ represents the global features related to PC_3 . Then $spots_g^3$ and $spots^2$ are aggregated to generate $spots_g^2$ with Point Fusion Block. Following the same method, the $spots_g^1$ is also obtained by $spots_g^2$ and $spots^1$. The $spots_g^3$, $spots_g^2$, $spots_g^1$ are aggregated in sequence to obtain point cloud P_{fine} with the Aggregation block.

As shown in Figure 7 (b), Point Fusion Block, as the key component of MPF, is denoted as the complete path and the refine path. The goal of the complete path is to generate a point cloud, and that of the refine path is to augment the reasoning of global features. In the complete path, $spots^m \in \mathbb{R}^{N_m \times C_m}$ ($m = 1, 2$) are used to generate $PC_m \in \mathbb{R}^{N_m \times 3}$. In the refine path, $spots_g^{m+1} \in \mathbb{R}^{N_{m+1} \times S_{m+1} \times C_{m+1}}$ represent N_{m+1} global features with S_{m+1} local features.

In order to refine these features, we reshape $spots_g^{m+1}$, and its shape becomes $[N_m, C_{m+1}] (N_m = N_{m+1} \times S_{m+1})$. Then applying MLP and reshaping on it obtains $S_m (S_m = N_m / N_{m+1})$ neighborhood information. In the end, $spots_g^m$ can be used to update itself by splicing intermediate features f from complete path and PC_m in channel dimension and then maps its dimension to the shape $[N_m, S_m, C_m]$. The formula is as follows:

$$spots_g^m = \phi(\phi(\nabla(\phi(\nabla(spots_g^{m+1})))) \cdot f \cdot PC_m) \quad (14)$$

where the letter “ ϕ ” means MLP, the letter “ ∇ ” indicates reshape operation. The “ \cdot ” is the symbol for concatenation.

3.6 Optimization

Due to the unordered property of point cloud, it may be difficult to directly measure the distance between the generated point cloud and the ground truth. For this issue, Fan et al. [2017] propose Chamfer Distance (CD) and Earth Mover’s Distance (EMD). We adopt Chamfer Distance as our loss function, because Chamfer Distance is more differentiable and more efficient than Earth Mover’s Distance [Huang et al., 2020]. We define Chamfer Distance can be given as:

$$cd(P_c, P_g) = \frac{1}{n_c} \sum_{c \in P_c} \min_{g \in P_g} \|c - g\|_2 + \frac{1}{n_g} \sum_{g \in P_g} \min_{c \in P_c} \|g - c\|_2 \quad (15)$$

where the symbol P_c represents the completed point cloud with n_c points, and the symbol P_g represents the ground truth with n_g points.

Our loss function consists of four items: cd_1 , cd_2 , cd_3 , and cd_{fine} . It is formulated:

$$\mathcal{L} = \alpha_1 cd_1(P_1, P_g) + \alpha_2 cd_2(P_2, P_g) + \alpha_3 cd_3(P_1, P_g) + \alpha_{fine} cd_{fine}(P_{fine}, P_g) \quad (16)$$

where α_1 , α_2 , α_3 , and α_{fine} are weights of our loss function. The value of α is illustrated in Section 4.2.

4 Experiment

In this section, we first introduce datasets for point cloud completion and the evaluation metric. Then we show results of point cloud completion for our models and other methods.

4.1 Dataset

PCN dataset is one of the most common datasets for point cloud completion, which created from ShapeNet [Wu et al., 2015] and published by PCN [Yuan et al., 2018]. PCN dataset is composed of 30974 CAD models from 8 categories. The train data is obtained by rendering the 28974 CAD model from 8 angles. The test data is obtained by rendering the 1200 CAD model from only 1 angle. Back-projecting a 2.5D depth image into a 3D point cloud obtains the incomplete data. The ground truth contains 16384 points.

MVP dataset is a new dataset for point cloud completion, which is presented by VRCNet [Pan et al., 2021]. Point clouds of MVP dataset are sampled by Poisson Disk Sampling from 4000 CAD models grouped into 16 categories. Both train data and test data are obtained by uniformly setting 26 angles to renders these CAD models. Therefore, the number of train data and test data are 2400×26 and 1600×26 .

4.2 Implementation Details

Details for CompletedT. We obtain three multi-resolution point clouds P_m , whose sizes N_m are 2048, 512 and 128, with IFPS. ResMLP mainly consists of the MLP Residual Block, having two MLP layers [64 – 64]. SGR gets $spots^m$ based on neighborhood points with SG. In Section 5.3, we conduct an ablation study to explore the influence of the number of neighborhood points and decide to set the number to 48. In addition to SG, an MLP layer with the parameter of C_{mlp} is needed to map the dimension of features of the low-resolution point cloud to that of the high-resolution point cloud. Then, the MLP Residual Block with four MLP layers $[(2 \times C_{mlp} + 2 \times 3) - C_{out} - C_{out} - C_{out}]$ and MaxPool are performed. Finally, an MLP layer with the parameter of $\frac{3 \times 16384}{N_m}$ is conducted. For three sampled point clouds P_1 , P_2 and P_3 , the features of P_1 is used to update that of P_2 , and then the updated features of P_2 is responsible

Table 1: Results of point cloud completion on PCN dataset in terms of per point Chamfer Distance $\times 10^4$ (lower is better).

Method	Airplane	Cabinet	Car	Chair	Lamp	Sofa	Table	Watercraft	Avg.
TopNet[Tchapmi et al., 2019]	2.25	5.21	3.66	6.13	7.27	6.86	4.60	4.59	5.07
PCN[Yuan et al., 2018]	1.74	4.27	2.79	4.79	5.39	5.49	3.53	3.36	3.92
MSN[Liu et al., 2020]	1.64	5.68	3.14	5.12	6.36	6.52	4.33	4.20	4.62
GRNet[Xie et al., 2020]	1.53	3.62	2.75	2.95	2.65	3.61	2.55	2.12	2.72
CompleteDT	1.02	3.94	2.42	2.91	2.08	4.03	2.26	1.83	2.56

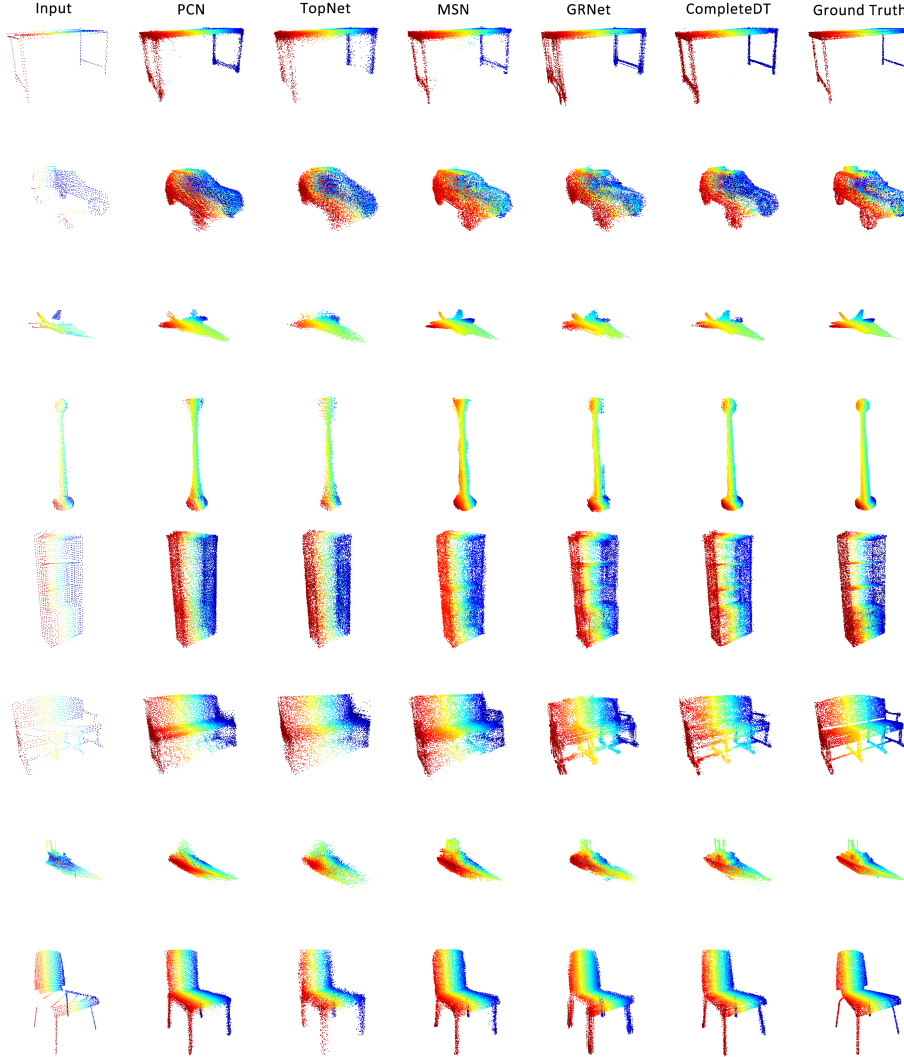


Figure 8: Visualization of point cloud completion on PCN dataset.

for the update of features of P_3 . Thus, we use SGR twice, where parameters of C_{mlp} are 64 and 128 in sequence, and parameters of MLP Residual Block are $[134 - 128 - 128 - 128]$ and $[262 - 256 - 256 - 256]$ sequentially. The important components of DRA are PLA and PDMA. PLA and PDMA receive $spots^m$. PLA learns local information adopting the attention mechanism, which has with four heads and each with a size of 64. PDMA consecutively uses multiple self-attention mechanism with four heads, and the dimension of each head is $64 \times sc_i (sc_1 = 2, sc_2 = 4)$. Both PLA and PDMA obtain the outputs with the dimension $[N_m, C_m]$, $C_m = \frac{3 \times 16384}{N_m}$. Then outputs are added together to update $spots$. Like SGR, DRA is used twice. Finally, MPF uses Spot Recovery Block to obtain $spots_g^3$ with the

shape of [128, 1, 384], and then uses the Point Fusion block to get $spots_g^2$ and $spots_g^1$, which shapes are [512, 4, 96] and [2048, 8, 24]. Based on these $spots_g$, a complete point cloud with 16384 resolution is generated. For the values of α_1 , α_2 , α_3 and α_{fine} in Section 3.6, we follow the parameter configuration of VRCNet[Pan et al., 2021], we set α_1 , α_2 and α_3 to 10, 0.5 and 0.5. For the first 5 epochs, 5-15 epochs and 15-30 epochs, we set α_{fine} to 0.01, 0.1 and 0.5. When epoch > 30 , $\alpha_{fine} = 1$.

Model configuration. Our CompleteDT is implemented using PyTorch. We train our models using the Adam optimizer with initial learning rate $1e^{-4}$ (decayed by 0.7 every 40 epochs) and batch size 32 by RTX 3090 GPU.

4.3 Point Cloud Completion on PCN dataset

Table 2: Results of point cloud completion on MVP dataset in terms of per point Chamfer Distance $\times 10^4$ (lower is better).

Method	Airplane	Cabinet	Car	Chair	Lamp	Sofa	Table	Watercraft	Bed	Bench	Bookshelf	Bus	Guitar	Motorbike	Pistol	Skateboard	Avg.
TopNet[Tchapmi et al., 2019]	2.65	4.44	3.68	8.87	14.14	5.74	7.04	6.05	10.42	5.62	7.33	2.75	1.45	4.27	4.77	2.54	5.74
PCN[Yuan et al., 2018]	3.04	4.08	3.12	7.85	14.73	5.40	7.11	5.64	12.01	5.32	7.16	2.55	1.15	3.55	3.91	2.17	5.55
MSN[Liu et al., 2020]	1.91	5.56	3.75	7.62	9.93	5.99	6.67	5.45	10.32	4.98	9.68	3.80	1.24	3.33	3.52	2.07	5.36
GRNet[Xie et al., 2020]	1.31	4.17	2.78	4.27	3.81	4.26	3.96	3.22	8.53	4.06	6.96	2.79	1.13	2.35	2.26	2.51	3.65
VRCNet[Pan et al., 2021]	1.15	3.2	2.14	3.58	5.57	3.58	4.17	2.47	6.90	2.76	3.45	1.78	0.59	1.52	1.83	1.57	2.90
CompleteDT	1.08	3.65	2.35	3.55	3.60	3.51	3.44	2.54	6.00	2.50	3.97	1.88	0.61	1.71	1.59	1.07	2.69

In this section, we compare the performance of our CompleteDT with other methods on the PCN dataset. We evaluate the results of point cloud completion in 16,384 resolution by adopting L2 metric of the chamfer distance. Compared with TopNet[Tchapmi et al., 2019], PCN[Yuan et al., 2018], MSN[Liu et al., 2020] and GRNet[Xie et al., 2020], the performance of CompleteDT is improved by 2.51, 1.36, 2.06, and 0.16, respectively. Since the experiments in this section are based on 16384 points, we follow GRNet[Xie et al., 2020] to combine the outputs of 2 times forward propagation to generate the point cloud with 16384 points. Table 1 proves that CompleteDT is superior to the other methods, and has a powerful ability to infer the complete shapes from incomplete shapes. The shapes shown in Figure 8 contain all categories of PCN dataset. We notice that some methods such as PCN,[Yuan et al., 2018] TopNet[Tchapmi et al., 2019] and MSN[Liu et al., 2020] introduces noise into the shape of Table (the first row). For the Airplane (the third row), the shape generated by TopNet[Tchapmi et al., 2019] is oversmoothed. Although PCN[Yuan et al., 2018] and GRNet[Xie et al., 2020] try to make details finer, they also form a point cloud while having noise. Contrary to these methods, each shape generated by our CompleteDT preserves the details of the input incomplete point cloud and infers the missing parts with rich information. For the shape of Watercraft, it clearly shows that our CompleteDT achieves the best performance in geometry and details compared to the over-smoothing caused by other models. Overall, these qualitative and quantitative results indicate that our CompleteDT generates better details of shapes (e.g., Watercrafts and Lamps) than the other methods.

4.4 Point Cloud Completion on MVP dataset

In this section, we show the experimental results of different methods on MVP dataset. From the table, we achieve the best performance on most objects and get the lowest average value of 2.69 (multiplied by 10^4). Compared to other methods, our performance improves by 3.05, 2.86, 2.67, 0.96 and 0.21 from Table 2. It is apparent from Figure 9 that our method generates shapes with more details than other methods do. CompleteDT achieves outstanding results while retaining consistent geometries with existing parts. Despite the increasing number of categories, CompleteDT still performs satisfactorily and its generalization ability is equally good. For some categories such as Lamp, Chair and Table, CompleteDT produces reliable shapes. Like legs of the Chair in the third row, MSN[Liu et al., 2020] tries its best to restore geometric details while generating a lot of noise. The point cloud generated by GRNet[Xie et al., 2020] using 3D voxels as the intermediation is noise-free but denser than the ground truth. However, the point cloud produced by our model is much closer to the ground truth.

5 Ablation Study

We further analyze the proposed CompleteDT through ablation studies based on the evaluation on PCN dataset and use the chamfer distance as the evaluation metric. In this section, we discuss (1) the advantage of modules in proposed methods; (2) the effectiveness of PDMA; (3) the number of neighborhood points.

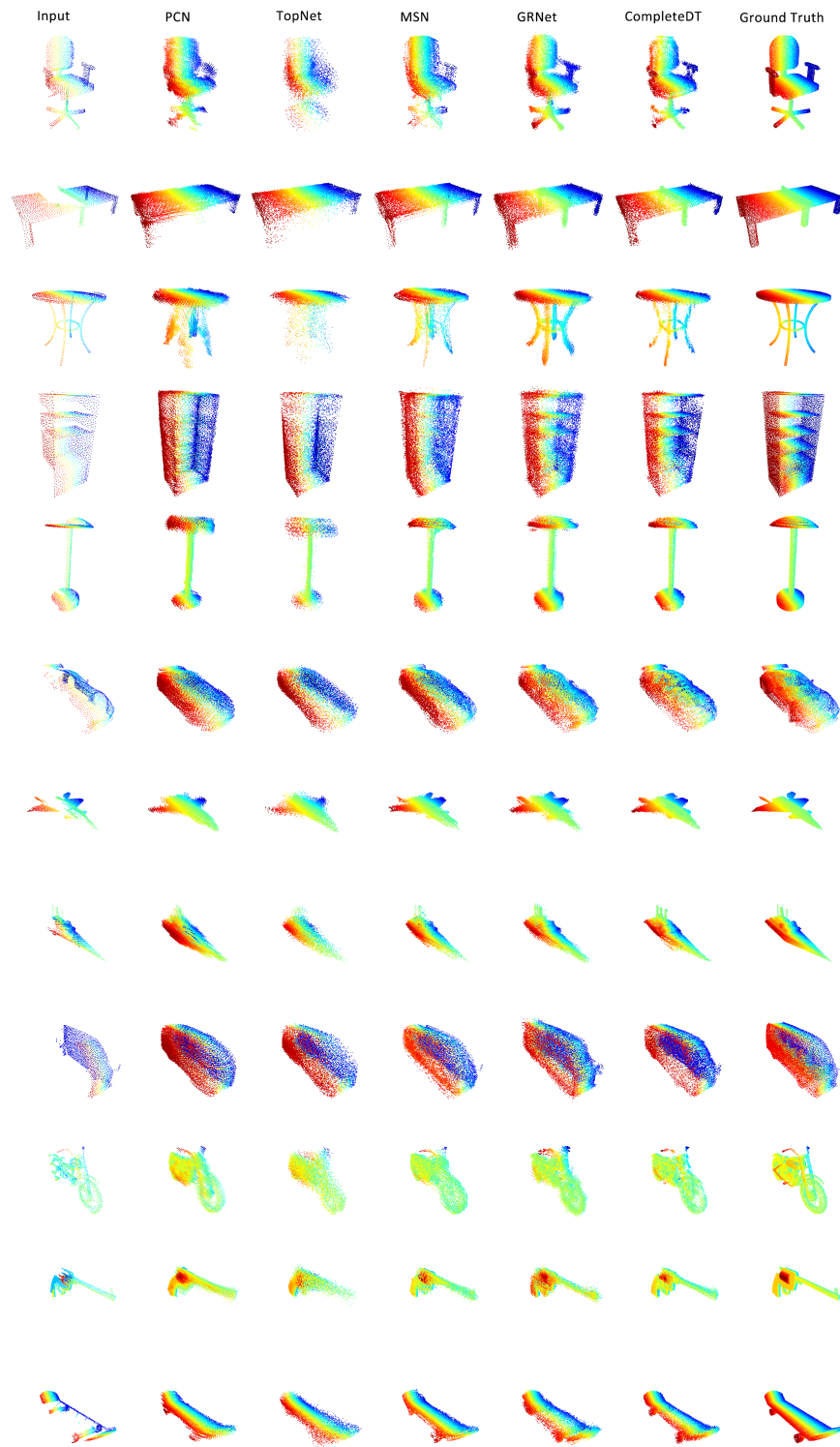


Figure 9: Visualization of point cloud completion on MVP dataset.

5.1 The validity of modules in CompleteDT

In this section, we investigate the validity of each module in the proposed CompleteDT. Recall that the CompleteDT is composed of four main modules: ResMLP, SGR, DRA and MPF. To verify the validity of above modules, we construct the following five networks. For the first network, it is used to assume that preprocessing operations can improve the performance of point cloud completion. It is composed of mentioned modules except ResMLP. The second network is used to prove the validity of SGR. Based on different resolution inputs, the SGR first obtains *spots* and then updates them. To demonstrate the effectiveness of SGR for reasoning in *spots*, we remove this module. Note that we temporarily supplement the acquisition process of *spots* to DRA, since in the original network DRA processes *spots* obtained from SGR. The third network contains mentioned modules except DRA. The fourth network is constructed by replacing MPF with MLP. The last network is the CompleteDT proposed. We evaluate the above networks on the PCN dataset with CD and their performance is listed in Table 3. From table, our CompleteDT (the last network) largely outperforms

Table 3: Results of ablation study about modules of CompleteDT in terms of per point Chamfer Distance $\times 10^4$ (lower is better).

Network	Module				CD (1×10^4)
	ResMLP	SGR	DRA	MPF	
1st	X	✓	✓	✓	3.09
2nd	✓	X	✓	✓	4.42
3rd	✓	✓	X	✓	3.10
4th	✓	✓	✓	X	3.79
5th	✓	✓	✓	✓	2.56

other networks by 0.53, 1.86, 0.54 and 1.23. According to the result of the first network, it confirms our hypothesis that ResMLP can help subsequent modules to transform features and achieve improved performance. The second network also proves the effectiveness of the self-guided approach. However, only relying on SGR to extract features may not achieve the best performance, and the third network demonstrates that DRA addresses such limitation. For the fourth network, the significant increase in CD underlines the importance of MPF. Experiments show that removing any module can reduce performance and CompleteDT works quantitatively.

5.2 The validity of DRA

Table 4: Results of ablation study about DRA in terms of per point Chamfer Distance $\times 10^4$ (lower is better)

PLA	PDMA			CD (1×10^4)
	Common transformer	No dense	Ours	
✓				3.00
			✓	2.83
✓			✓	2.56
✓	✓			2.70
✓		✓		2.65

In Section 5.1, we discussed the undesirable performance without DRA, now we further analyze components of DRA. DRA consisting of PLA and PDMA is an important module to augment feature extraction. While completing the point cloud benefits from either PLA or PDMA, the combination between them is much important. Here we investigate whether combining them results in improved performance. As shown in Table 4, combining PLA and PDMA results in a modest boost in the performance of point cloud completion, while using PLA or PDMA individually suffers a performance drop of 0.43 or 0.26 (the first two rows). Figure 10 indicates the visualization of feature weights mapped to the original point cloud. The lighter the color, the more important the learned feature is. The left of Figure 10 shows two point clouds of different resolutions from SGR, and the right of Figure 10 shows the visualization of features from PLA (the green arrow), PDMA (the blue arrow), and combined PLA and PDMA (the black arrow). It is apparent from Figure 10 that (1) PLA responds well to structures with obvious geometries, thanks to the enhanced inference of local features; (2) Different from PLA, PDMA provides opportunities for long-range interaction and therefore focuses on the global information. (3) The most striking result is that the combination of PLA and PDMA can both focus on global information and learn useful local features for geometric structures.

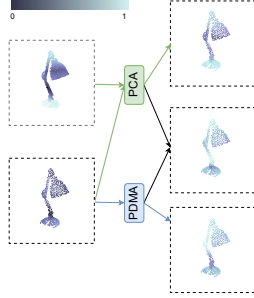


Figure 10: Visualization of feature weights mapped to the original point cloud.

PDMA is one of the core modules of our CompleteDT and is well worth discussing deeply. Our PDMA processes features by taking the multi-scale attention allied with the dense connection. We provide the network where replacing PDMA with the common transformer[Vaswani et al., 2017] or multi-scale attention. From Table 4, it is worth noting that while it performs 0.14 and 0.09 worse than our CompleteDT, the multi-scale attention still leads to better results than the some SOTA methods like GRNet[Xie et al., 2020].

5.3 The number of neighbors of the *spot*

After obtaining *spots* containing local information based on neighbors between multi-resolution point clouds through SGR, PLA in DRA can update *spots* within these neighbors, and PDMA in DRA provides opportunities for interaction among these *spots*. Based on the above design, the number of neighbors is positively related to the performance and the computational cost of CompleteDT, so an appropriate number of neighbors is especially important for representing *spots*. Specifically, a large number of neighbors may not improve performance, but may result in complex computations; only a few neighbors may fail to extract local features effectively resulting in poor performance. Thus, we conduct an ablation study on PCN dataset about the number S of grouped neighborhood points, which $S=16,24,48$ and 96. As shown in Table 5, we compare the properties of models, like their sizes (number of parameters (Params)) and computational cost (floating point operations required (FLOPs)), on a single object.

Table 5: Results of ablation study about the number S of neighbors in terms of per point Chamfer Distance $\times 10^4$ (lower is better)

S	Params (M)	FLOPs (G)	CD (1×10^4)
16	40.27	4.43	2.73
24	40.27	5.30	2.63
48	40.27	7.90	2.56
96	40.27	13.10	2.58
128	40.27	16.56	2.60

From Table 5, the chamfer distance of CompleteDT is better than that of other networks by 0.17, 0.07, 0.02 and 0.04, respectively. A small number of neighbors lead to an unsatisfactory expectation since missing local information, while a large number of neighbors result in increased computational cost. To balance computational cost and performance, we set the number of neighbors to 48.

6 Conclusion

In this paper, CompleteDT is designed to determine 3D geometric knowledge for completing point cloud. CompleteDT consists of ResMLP, SGR, DRA and MPF. ResMLP is a feature pre-extractor that lays the foundation for the performance of subsequent modules. SGR first collects local information to generate *spots*, and then DRA is available for enhancing the reasoning of *spots*. To be specific, DRA, a novel transformer-based module including PLA and PDMA, is proposed for augmenting the inference of features extraction. PLA facilitates the extraction of information with each *spot*, and PDMA effectively provides global correlation between *spots*. Finally, MPF generates high-quality complete point clouds in the way to update features with the help of points. Evaluations on PCN dataset and MVP dataset show that CompleteDT based on the above modules gets more expressive features to complete shapes and outperforms some state-of-the-art methods.

References

- Zitian Huang, Yikuan Yu, Jiawen Xu, Feng Ni, and Xinyi Le. Pf-net: Point fractal network for 3d point cloud completion. In *Proceedings of the IEEE/CVF Conference on Computer Vision and Pattern Recognition*, pages 7662–7670, 2020.
- Charles R Qi, Hao Su, Kaichun Mo, and Leonidas J Guibas. Pointnet: Deep learning on point sets for 3d classification and segmentation. In *Proceedings of the IEEE conference on computer vision and pattern recognition*, pages 652–660, 2017a.
- Charles Ruizhongtai Qi, Li Yi, Hao Su, and Leonidas J Guibas. Pointnet++: Deep hierarchical feature learning on point sets in a metric space. *Advances in neural information processing systems*, 30, 2017b.
- Huan Lei, Naveed Akhtar, and Ajmal Mian. Seggcn: Efficient 3d point cloud segmentation with fuzzy spherical kernel. In *Proceedings of the IEEE/CVF Conference on Computer Vision and Pattern Recognition*, pages 11611–11620, 2020.
- Xun Xu and Gim Hee Lee. Weakly supervised semantic point cloud segmentation: Towards 10x fewer labels. In *Proceedings of the IEEE/CVF conference on computer vision and pattern recognition*, pages 13706–13715, 2020.
- Waleed Ali, Sherif Abdelkarim, Mahmoud Zidan, Mohamed Zahran, and Ahmad El Sallab. Yolo3d: End-to-end real-time 3d oriented object bounding box detection from lidar point cloud. In *Proceedings of the European Conference on Computer Vision (ECCV) Workshops*, pages 0–0, 2018.
- Xiaozhi Chen, Huimin Ma, Ji Wan, Bo Li, and Tian Xia. Multi-view 3d object detection network for autonomous driving. In *Proceedings of the IEEE conference on Computer Vision and Pattern Recognition*, pages 1907–1915, 2017.
- Angela Dai, Charles Ruizhongtai Qi, and Matthias Nießner. Shape completion using 3d-encoder-predictor cnns and shape synthesis. In *Proceedings of the IEEE conference on computer vision and pattern recognition*, pages 5868–5877, 2017.
- Bo Yang, Hongkai Wen, Sen Wang, Ronald Clark, Andrew Markham, and Niki Trigoni. 3d object reconstruction from a single depth view with adversarial learning. In *Proceedings of the IEEE International Conference on Computer Vision Workshops*, pages 679–688, 2017.
- Priyanka Mandikal and Venkatesh Babu Radhakrishnan. Dense 3d point cloud reconstruction using a deep pyramid network. In *2019 IEEE Winter Conference on Applications of Computer Vision (WACV)*, pages 1052–1060. IEEE, 2019.
- Wentao Yuan, Tejas Khot, David Held, Christoph Mertz, and Martial Hebert. Pcn: Point completion network. In *2018 International Conference on 3D Vision (3DV)*, pages 728–737. IEEE, 2018.
- Panos Achlioptas, Olga Diamanti, Ioannis Mitliagkas, and Leonidas Guibas. Learning representations and generative models for 3d point clouds. In *International conference on machine learning*, pages 40–49. PMLR, 2018.
- Thibault Groueix, Matthew Fisher, Vladimir G Kim, Bryan C Russell, and Mathieu Aubry. A papier-mâché approach to learning 3d surface generation. In *Proceedings of the IEEE conference on computer vision and pattern recognition*, pages 216–224, 2018.
- Muhammad Sarmad, Hyunjoo Jenny Lee, and Young Min Kim. Rl-gan-net: A reinforcement learning agent controlled gan network for real-time point cloud shape completion. In *Proceedings of the IEEE/CVF Conference on Computer Vision and Pattern Recognition*, pages 5898–5907, 2019.
- Xiaogang Wang, Marcelo H Ang Jr, and Gim Hee Lee. Cascaded refinement network for point cloud completion. In *Proceedings of the IEEE/CVF Conference on Computer Vision and Pattern Recognition*, pages 790–799, 2020a.
- Xin Wen, Tianyang Li, Zhizhong Han, and Yu-Shen Liu. Point cloud completion by skip-attention network with hierarchical folding. In *Proceedings of the IEEE/CVF Conference on Computer Vision and Pattern Recognition*, pages 1939–1948, 2020.
- Xin Wen, Peng Xiang, Zhizhong Han, Yan-Pei Cao, Pengfei Wan, Wen Zheng, and Yu-Shen Liu. Pmp-net: Point cloud completion by learning multi-step point moving paths. In *Proceedings of the IEEE/CVF Conference on Computer Vision and Pattern Recognition*, pages 7443–7452, 2021.
- Liang Pan. Ecg: Edge-aware point cloud completion with graph convolution. *IEEE Robotics and Automation Letters*, 5(3):4392–4398, 2020.
- Ashish Vaswani, Noam Shazeer, Niki Parmar, Jakob Uszkoreit, Llion Jones, Aidan N Gomez, Łukasz Kaiser, and Illia Polosukhin. Attention is all you need. *Advances in neural information processing systems*, 30, 2017.
- Yida Wang, David Joseph Tan, Nassir Navab, and Federico Tombari. Forknet: Multi-branch volumetric semantic completion from a single depth image. In *Proceedings of the IEEE/CVF International Conference on Computer Vision*, pages 8608–8617, 2019.

- Xiaoguang Han, Zhen Li, Haibin Huang, Evangelos Kalogerakis, and Yizhou Yu. High-resolution shape completion using deep neural networks for global structure and local geometry inference. In *Proceedings of the IEEE international conference on computer vision*, pages 85–93, 2017.
- Duc Thanh Nguyen, Binh-Son Hua, Khoi Tran, Quang-Hieu Pham, and Sai-Kit Yeung. A field model for repairing 3d shapes. In *Proceedings of the IEEE Conference on Computer Vision and Pattern Recognition*, pages 5676–5684, 2016.
- David Stutz and Andreas Geiger. Learning 3d shape completion from laser scan data with weak supervision. In *Proceedings of the IEEE Conference on Computer Vision and Pattern Recognition*, pages 1955–1964, 2018.
- Jacob Varley, Chad DeChant, Adam Richardson, Joaquín Ruales, and Peter Allen. Shape completion enabled robotic grasping. In *2017 IEEE/RSJ international conference on intelligent robots and systems (IROS)*, pages 2442–2447. IEEE, 2017.
- Liang Pan, Xinyi Chen, Zhongang Cai, Junzhe Zhang, Haiyu Zhao, Shuai Yi, and Ziwei Liu. Variational relational point completion network. In *Proceedings of the IEEE/CVF Conference on Computer Vision and Pattern Recognition*, pages 8524–8533, 2021.
- Haozhe Xie, Hongxun Yao, Shangchen Zhou, Jiageng Mao, Shengping Zhang, and Wenxiu Sun. Grnet: Gridding residual network for dense point cloud completion. In *European Conference on Computer Vision*, pages 365–381. Springer, 2020.
- Yida Wang, David Joseph Tan, Nassir Navab, and Federico Tombari. Softpoolnet: Shape descriptor for point cloud completion and classification. In *European Conference on Computer Vision*, pages 70–85. Springer, 2020b.
- Yida Wang, David Joseph Tan, Nassir Navab, and Federico Tombari. Softpool++: An encoder–decoder network for point cloud completion. *International Journal of Computer Vision*, 130(5):1145–1164, 2022.
- Jacob Devlin, Ming-Wei Chang, Kenton Lee, and Kristina Toutanova. Bert: Pre-training of deep bidirectional transformers for language understanding. *arXiv preprint arXiv:1810.04805*, 2018.
- Ze Liu, Yutong Lin, Yue Cao, Han Hu, Yixuan Wei, Zheng Zhang, Stephen Lin, and Baining Guo. Swin transformer: Hierarchical vision transformer using shifted windows. In *Proceedings of the IEEE/CVF International Conference on Computer Vision*, pages 10012–10022, 2021.
- Yongming Rao, Wenliang Zhao, Benlin Liu, Jiwen Lu, Jie Zhou, and Cho-Jui Hsieh. Dynamicvit: Efficient vision transformers with dynamic token sparsification. *Advances in neural information processing systems*, 34, 2021.
- Meng-Hao Guo, Jun-Xiong Cai, Zheng-Ning Liu, Tai-Jiang Mu, Ralph R Martin, and Shi-Min Hu. Pct: Point cloud transformer. *Computational Visual Media*, 7(2):187–199, 2021.
- Xin Wen, Peng Xiang, Zhizhong Han, Yan-Pei Cao, Pengfei Wan, Wen Zheng, and Yu-Shen Liu. Pmp-net++: Point cloud completion by transformer-enhanced multi-step point moving paths. *IEEE Transactions on Pattern Analysis and Machine Intelligence*, 2022.
- Xumin Yu, Yongming Rao, Ziyi Wang, Zuyan Liu, Jiwen Lu, and Jie Zhou. Pointr: Diverse point cloud completion with geometry-aware transformers. In *Proceedings of the IEEE/CVF International Conference on Computer Vision*, pages 12498–12507, 2021.
- Yiming Cui, Xin Liu, Hongmin Liu, Jiyong Zhang, Alina Zare, and Bin Fan. Geometric attentional dynamic graph convolutional neural networks for point cloud analysis. *Neurocomputing*, 432:300–310, 2021.
- Gao Huang, Zhuang Liu, Laurens Van Der Maaten, and Kilian Q Weinberger. Densely connected convolutional networks. In *Proceedings of the IEEE conference on computer vision and pattern recognition*, pages 4700–4708, 2017.
- Forrest Iandola, Matt Moskewicz, Sergey Karayev, Ross Girshick, Trevor Darrell, and Kurt Keutzer. Densenet: Implementing efficient convnet descriptor pyramids. *arXiv preprint arXiv:1404.1869*, 2014.
- Yongcheng Liu, Bin Fan, Gaofeng Meng, Jiwen Lu, Shiming Xiang, and Chunhong Pan. Densepoint: Learning densely contextual representation for efficient point cloud processing. In *Proceedings of the IEEE/CVF International Conference on Computer Vision*, pages 5239–5248, 2019.
- Haoqiang Fan, Hao Su, and Leonidas J Guibas. A point set generation network for 3d object reconstruction from a single image. In *Proceedings of the IEEE conference on computer vision and pattern recognition*, pages 605–613, 2017.
- Zhirong Wu, Shuran Song, Aditya Khosla, Fisher Yu, Linguang Zhang, Xiaoou Tang, and Jianxiong Xiao. 3d shapenets: A deep representation for volumetric shapes. In *Proceedings of the IEEE conference on computer vision and pattern recognition*, pages 1912–1920, 2015.

Lyne P Tchapmi, Vineet Kosaraju, Hamid Rezatofghi, Ian Reid, and Silvio Savarese. Topnet: Structural point cloud decoder. In *Proceedings of the IEEE/CVF Conference on Computer Vision and Pattern Recognition*, pages 383–392, 2019.

Minghua Liu, Lu Sheng, Sheng Yang, Jing Shao, and Shi-Min Hu. Morphing and sampling network for dense point cloud completion. In *Proceedings of the AAAI conference on artificial intelligence*, volume 34, pages 11596–11603, 2020.